Underwater Biomimetic Lateral Line Sensor Based on Triboelectric Nanogenerator for Dynamic Pressure Monitoring and Trajectory Perception

Jianhua Liu, Peng Xu,* Bo Liu, Ziyue Xi, Yuanzheng Li, Linan Guo, Tangzhen Guan, Peng Zhu, Zhaochen Meng, Siyuan Wang, Hao Wang,* and Minyi Xu*

Developing desirable sensors is crucial for underwater perceptions and operations. The perceiving organs of marine creatures have greatly evolved to react accurately and promptly underwater. Inspired by the fish lateral line, this study proposes a triboelectric dynamic pressure sensor for underwater perception. The biomimetic lateral line sensor (BLLS) has high sensitivity to the disturbance amplitude/frequency, good adaptability to underwater environments and (relative) low cost. The sensors are deployed at the bottom of the test basin to perceive various moving objects, such as a robotic fish, robotic seal, etc. By analyzing the electrical signal of the sensor, the motion parameters of the objects passed over can be obtained. By monitoring signal variations across multiple sensors, the ability to sense different disturbance movement trajectories, including linear and angular trajectories, is achievable. The study will prove significant in forming an unconventional underwater perceiving method, which can back-up the sonic/optical sensors when are impaired in complex underwater environments.

1. Introduction

Complex marine environments are always posing great challenges for underwater perception. Traditional underwater perception methods (sonic/optical) are frequently impaired in turbid/dark underwater environments.[1–3] Meanwhile, the underwater perception equipment also suffers from heavy cost for maintenance and replacement,[4,5] which are the bottleneck in realizing effective, reliable underwater perception. Therefore, it is especially critical to develop an underwater sensor that can continuously function in complex underwater environments. Marine creatures have acquired agile sensing capabilities through generations of evolution, which helps them perceive the fluid field[6,7] as well as the preys/predators.[8–10] The blind cavefish has impaired vision and relies more on its lateral line to perceive the surrounding moving objects.[11–13] Researchers have developed various artificial lateral line sensors based on piezoresistive, piezoelectric, and capacitive mechanisms.[14,15] In particular, Jiang et al. have developed a sensor based on piezoelectric nanofiber materials with photolithography.[16] The detection range of this sensor is enhanced by a preamplifier. Kottapalli et al. proposed an artificial micro electro mechanical systems (MEMS) sensor consisting of a piezoelectric MEMS sensing membrane, high-aspect-ratio hair cells, and a biomimetic canal housing the sensor.[17] The performance of the artificial canal sensor clearly reflects the ability to eliminate low-frequency noise. However, these sensors require a rather complex preparation process.

As an emerging technology, triboelectric nanogenerator plays a growing role in marine energy harvesting[18–25] and marine distributed sensing,[26–30] such as in offshore platforms monitoring,[31] in wave information measurement,[32] and in ship engine/equipment maintenance.[33] Sensors based on triboelectric nanogenerator can perceiving a variety of information and trigger alarm as necessary.[34–38] Moreover, it has the advantages of abundant alternative materials (including flexible materials),[39–41] low production costs[42] and good robustness. Therefore, developing high performance sensors with triboelectric nanogenerator could create a new, effective perceiving method underwater.

In this study, based on the mechanism of triboelectric nanogenerator, a biomimetic lateral line sensor (BLLS) is designed to perceive the dynamic pressure underwater. The core unit of the sensor is manufactured with fluorinated ethylene propylene

J. Liu, P. Xu, B. Liu, Z. Xi, Y. Li, L. Guo, T. Guan, P. Zhu, Z. Meng, S. Wang, H. Wang, M. Xu
Dalian Key Lab of Marine Micro/Nano Energy and Self-powered Systems, Marine Engineering College
Dalian Maritime University
Dalian 116026, China
E-mail: pengxu@pku.edu.cn; hao8901@dlmu.edu.cn; xuminyi@dlmu.edu.cn
P. Xu
Intelligent Biomimetic Design Lab, College of Engineering
Peking University
Beijing 100871, China
T. Guan
Liquid Metal and Cryogenic Biomedical Research Center
Technical Institute of Physics and Chemistry
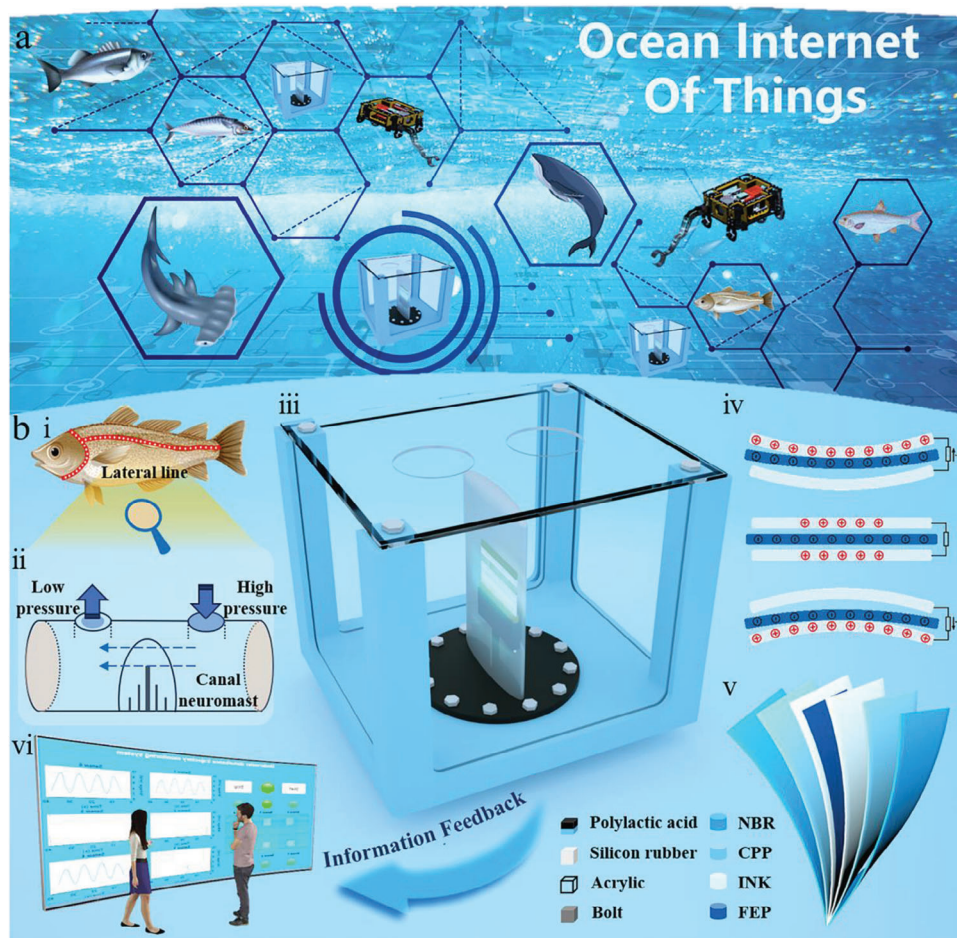Chinese Academy of Sciences
Beijing 100190, China

Figure 1. Application scenarios and working principles of BLLS. a) Schematic diagram of underwater perception. b-i) Surface lateral lines of the fish. b-ii) Perception mechanism of canal neuromast. b-iii) Structure diagram of the BLLS. b-iv) Perception principle diagram of the BLLS. b-v) Material composition of the sensing unit. b-vi) Information (from the BLLS) display.

(FEP) of strong electronegativity, along with conductive ink of strong electropositive. Covered with nitrile butadiene rubber (NBR) of good wear resistance, it is embedded in silicone material for waterproof packaging. The sensor is sealed in an acrylic cover to minimize wear and damage. Through a series of experiments and demonstrations, it is found that the sensor could respond to the pressure difference between the inlet and outlet, so as to effectively perceive the external disturbance. Taking advantage of high sensitivity, good adaptability and the (relative) low cost of the triboelectric nanogenerator, the sensor has shown its superiority in underwater perception. It will also contribute to the rapid development of the ocean IoT, as shown in **Figure 1**a.

2. Design and Working Principle of BLLS

As one of the most populous species, fish is equipped with impressive perception capabilities underwater.[43–45] As shown in Figure 1b-i, the lateral line are distributed on their bodies, which is of great significance to the decision-making of fish. One part of the sensing unit is called the canal neuromast, and the apex of all hair cells in the canal neuromast will protrude into a transparent glial apex.[46] It is extremely sensitive to pressure variations,

as shown in Figure 1b-ii. When the fish perceives disturbances, the glial top will deflect and transmit to the cilia, triggering the ion to pass through the hair cell membrane. In the process, the signals travel via afferents to the central nervous system.[47] In this way, fish can perceive the mechanical disturbances through the lateral line, and then respond quickly to complete behaviors such as predation or escape.

Inspired by the neuromast structure of the lateral line, this study designs a bionic lateral line dynamic pressure sensor ($L = 140.0$ mm, $w = 140.0$ mm, $H = 155.0$ mm). Figure 1b-iii shows the structure of the sensor, which is composed by a polylactic acid (PLA) base with good biodegradability, a PLA connecting pads, a side plate made of transparent acrylic and a top plate with water inlet and outlet ($r = 20.0$ mm). The sensing unit is encapsulated by silicone. The material composition inside the sensing unit is shown in Figure 1b-v. It includes a highly electropositive conductive ink and a strongly electronegative FEP. Its outer layer is covered with cast polypropylene (CPP) that can shield electrostatic interference. NBR with good wear resistance and strong adhesion can effectively improve the working life of the BLLS.

Figure 1b-iv demonstrates its charge transfer process. When the external flow field varies, a pressure difference will form
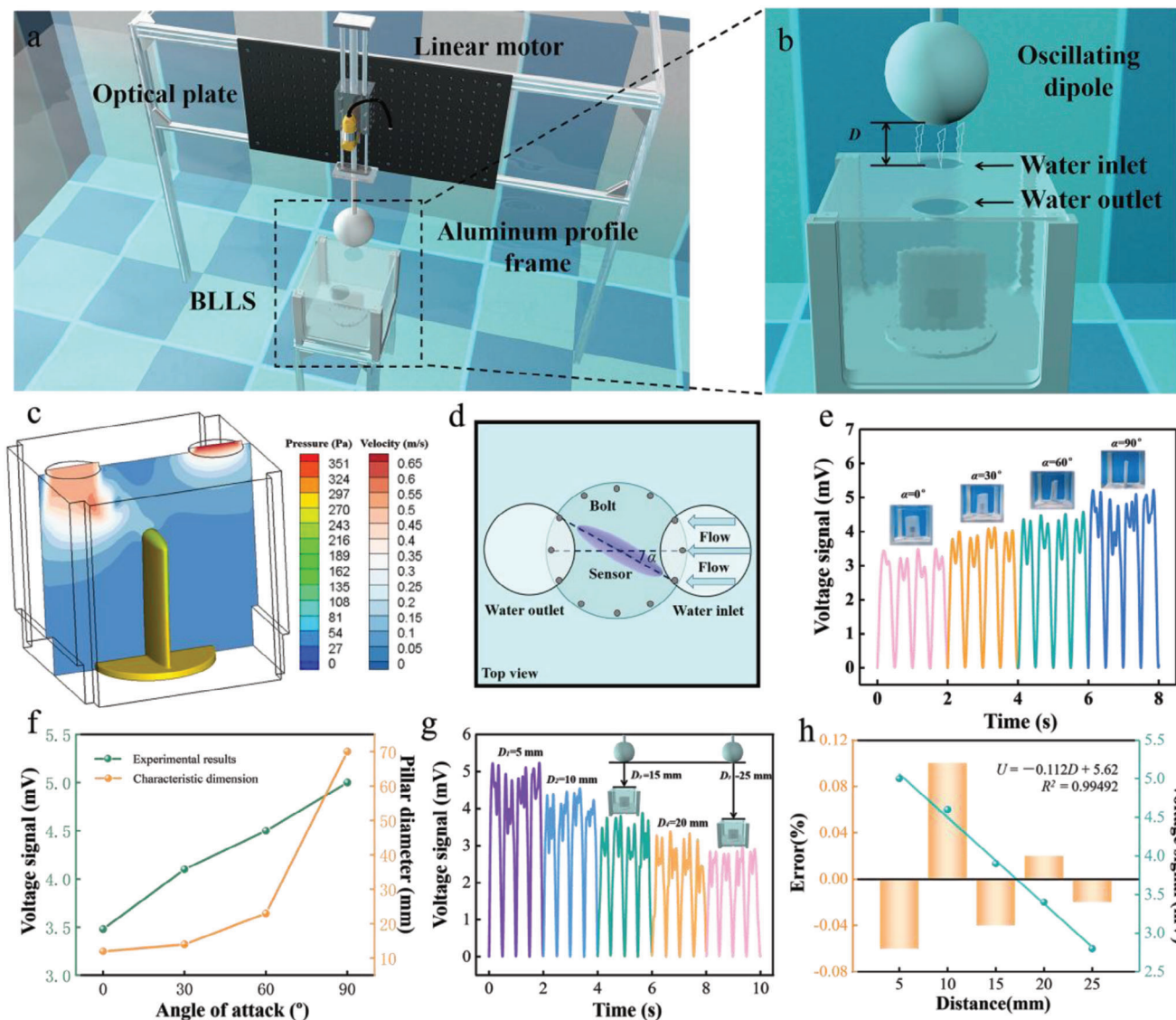
**ADVANCED
SCIENCE NEWS**

www.advancedsciencenews.com

NANO · MICRO

small

www.small-journal.com

Figure 2. Test devices and measured data of the BLLS. a) Test device for the BLLS. b) A schematic view of the BLLS experiment. c) The ANSYS simulation for the BLLS. d) Schematic diagram of the angle of attack of the BLLS. e) The open-circuit voltage corresponding to the angle of attack from 0° to 90°. f) The voltage signal and the effective diameter, with respect to the angle of attack. g) Variations of the open-circuit voltage with respect to the external displacement from 5.0 to 25.0 mm. h) Linear fitting between the open-circuit voltage and the external distance.

between the inlet and outlet of the BLLS. Corresponding to that, the internal sensing unit will deflect. The FEP inside the sensing unit contacts the conductive ink electrode on one side, obtaining opposite charges on the surfaces of the two materials through the triboelectric effect. The surface of FEP is negatively charged while the conductive ink is positively charged. When the disturbance is neutralized, the sensing unit returns to its initial state, and the dielectric layer is separated from the electrode layer. Since the electrons in the external circuit flow from one side of the electrode to the other, the opposite electrode becomes positively charged balancing the potential difference. As the dielectric layer moves toward the electrode layer on the other side, the charge is completely transferred. In the final stage, as the FEP returns to neutral state, the charge transfers reversely, producing an output with opposite phase. To better present the

working principle of the BLLS, COMSOL software is used to simulate the charge transfer, as shown in Figure. S2 (Supporting Information). The corresponding electrical signal generated is measured by the system shown in Figure 1b-vi.

3. Results and Discussion

To explore the perception performance of the BLLS underwater, a test platform is designed, as shown in **Figure 2**a. The platform adopts an aluminum frame to hold the optical plate. The linear motor is mounted on the optical plate. And a spherical oscillating dipole (fabricated by a 3D printer) is mounted at the lower end of the linear motor. Figure 2b depicts the vertical oscillation of the spherical oscillating dipole above the inlet of the BLLS. The shortest distance between the water inlet and the dipole is D. The BLLS

could perceive the dynamic pressures variation as the spherical oscillating dipole oscillates. The signal acquisition device transmits the signal to the processing terminal, which will be displayed in real time. Figure 2c shows the simulation of the BLLS structure using ANSYS, in which the response of the perception unit of the BLLS under disturbance is demonstrated. As the inlet and outlet of the BLLS yield different flow rates, the pressure difference acts on the surface of the silicone and makes it bend, so that the sensing unit inside generates the corresponding signal. Three kinds of silicone rubber materials with different Shore hardness have been compared in the study, as shown in Figure S3 (Supporting Information). As the Shore hardness decreases, the open-circuit voltage signal of the sensing unit increases. Among them, the Ecoflex20 material produces an open-circuit voltage of 5.0 mV, which superior to other materials. Therefore, it is selected in the rest of the study.

A connection plate that can rotate is designed to explore the effect of the angle of attack of the sensing unit on the perception performance. Figure 2d is the top view depicting the angle of attack of the sensing unit. Within the BLLS, the fluid flows from the inlet to the outlet. The angle between the major diameter of the elliptical sensing unit and the flow direction is the angle of attack α. With an oscillation frequency of 2.0 Hz and a distance of 5.0 mm, a series of tests are carried out under different angles of attack. Figure 2e depicts the open-circuit voltage of the BLLS with respect to the angle of attack, and the corresponding front views of the sensing unit under different angles of attack. The open-circuit voltage of the BLLS is 3.5 mV when the angle of attack of the sensing unit is 0°. As the angle of attack increases to 90°, the open-circuit voltage of the BLLS increases to 5.0 mV. This is because when the angle of attack of the sensing unit is small, the deformation caused by the impact of the water flow is relatively small. The contact area of the internal friction material is limited, so the amount of charge transfer is not large. As the angle of attack increases to 90°, the conductive ink inside the sensing unit is fully in contact with the FEP. The amount of charge transfer increases accordingly, generating larger output signal. Therefore, the BLLS is further analyzed when the angle of attack is set to 90°. Figure 2f depicts the open-circuit voltage and effective diameter of the BLLS with respect to the angle of attack. The effective diameter is determined by the angle of attack:

$$D_p = D_L \, D_s \sqrt{\frac{1 + cot^2(\alpha)}{D_s^2 + D_L^2 cot^2(\alpha)}} \tag{1}$$

D_L is the major diameter of the elliptical sensing unit, D_s is the minor diameter of the elliptical sensing unit. When the angle of attack is 0°, the effective diameter of the sensing unit in the normal direction of water flow is 12.0 mm. As the angle of attack increases, the effective diameter of the sensing unit gradually increases, until it reaches the maximum value of 70.0 mm. Meanwhile, with the increase of the angle of attack, the open-circuit voltage of the BLLS increases, and the two yield a quite linear correlation. Figure S4 (Supporting Information) shows the linear fitting between the two: $U = 0.01653A + 3.526$, and the linear correlation coefficient $R^2 = 0.98944$. It can be seen that when the angle of attack is 90°, the perception of the BLLS reaches optimal.

Next, the variation of the BLLS output with respect to the distance between the dipole and the water inlet is studied. The oscillation frequency of the dipole is set to 2.0 Hz, as shown in Figure 2g. The open-circuit voltage signal of the BLLS is 5.0 mV when the dipole is 5.0 cm from the water inlet. The open-circuit voltage signal of the BLLS decreases to 2.7 mV with the distance increasing to 25.0 mm. Figure 2h uses the leave-one-out cross-validation (LOOCV) strategy to obtain the relationship between the open-circuit voltage and the distance of the external dipole: $U = -0.112D + 5.62$, $R^2 = 0.99492$. When the dipole is 10.0 mm from the water inlet, the error is up to 0.1%. The lowest error is 0.02% when the distance is 20.0 mm.

The response of the BLLS to disturbances is explored by measuring the signal accompanying the spherical oscillating dipole during one cycle of motion, as shown in **Figure 3**a. As the dipole moves toward the BLLS, the electrical signal generated by the sensing unit yields a rising edge, and the response time is ≈0.15 s. When the dipole moves away from the BLLS, the voltage signal yields a falling edge, for ≈0.11 s. It shows that the BLLS has the characteristics of sensitive response to external excitations. Figure S5 (Supporting Information) clearly shows the state changes of the sensing unit during the movement of the oscillating dipole. Generally speaking, there are a variety of disturbances underwater, producing a variety of output signals. To examine the perception ability of the BLLS to different disturbance, different oscillation frequencies were tested (when D is set to 5.0 mm). The oscillation frequency of the dipole is determined by setting the parameters of the linear motor.

As shown in Figure 3b, the open-circuit voltage generated by the BLLS is ≈1.8 mV when the dipole oscillation frequency is 1.0 Hz. As the oscillation frequency generated by the dipole increases, the open-circuit voltage yields an increasing trend. As the oscillation frequency increases to 2.0 Hz, the open-circuit voltage of the BLLS reaches a maximum of 5.0 mV. It shows that with increased frequency, the response to the external disturbance enhances. As the dynamic pressure amplitude exciting the sensing unit increases, the signal strength increases. The relationship between the open-circuit voltage and the oscillation frequency of the external dipole has been obtained by leave-one-out cross-validation (LOOCV) strategy, as shown in Figure 3c: $U = 3.21622f - 1.4973$. The linear correlation coefficient $R^2 = 0.99604$. This proves that the BLLS has good ability to perceive the disturbance frequency. Figure 3d has presented the open-circuit voltage of the BLLS with respect to the distance and with respect to the frequency. It can be found that the BLLS is more sensitive to frequency variations.

The study also explores the effect of the diameter of the oscillating dipole on the open-circuit voltage of the BLLS, as shown in Figure 3e. Four dipoles with different diameter sizes are tested under a frequency of 2.0 Hz and a distance of 5.0 mm, as shown in Figure S6 (Supporting Information). The open-circuit voltage generated by the BLLS when the dipole diameter is 8.0 cm is ≈3.7 mV. The open-circuit voltage of the BLLS increases with the increasing diameter of the dipole. The open-circuit voltage is ≈5.3 mV when tested with a dipole with a diameter of 14.0 cm. When the dipole diameter is 10.0 cm, the linear fitting error is 0.07%. When the dipole diameter is 12.0 cm, the linear fitting error is 0.13%. This means that the BLLS' output can be used to estimate the volume of the oscillating dipole.
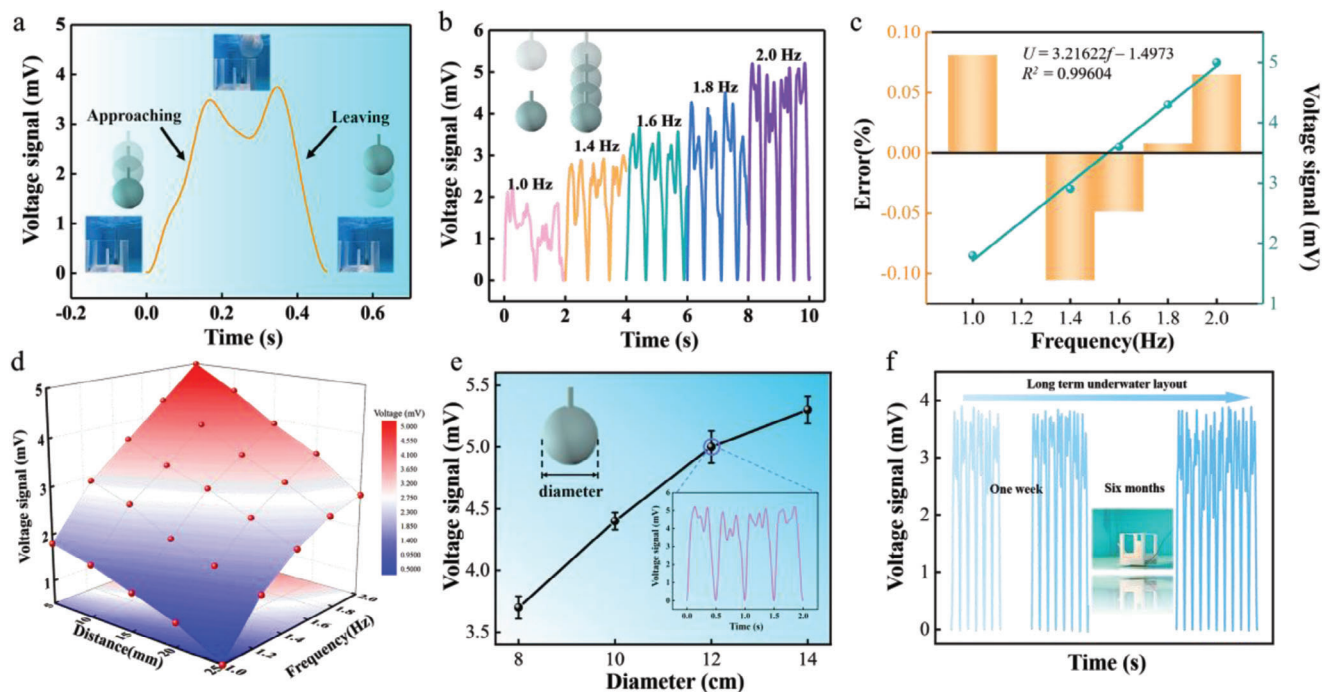
**ADVANCED
SCIENCE NEWS**

www.advancedsciencenews.com

NANO · MICRO

small

www.small-journal.com

Figure 3. Experimental data analysis of the BLLS. a) Response time of the voltage signal of the BLLS to external stimuli. b) The open-circuit voltage under the frequency of 1.0 to 2.0 Hz. c) Linear fitting between the open-circuit voltage and the frequency. d) The distribution of the open circuit voltage with respect to the distance and the frequency. e) The open-circuit voltage with respect to diameter of dipole (from 8.0 to 14.0 mm). f) Durability test of the BLLS.

As the BLLS is designed to work underwater for a long time, the BLLS is placed underwater to test its durability, as depicted in Figure 3f. It can be seen that the initial open-circuit voltage of the BLLS is ≈5.0 mV. After 1 week, the voltage output signal (under the same test conditions) remained very close to 5.0 mV. Subsequently, after 6 months, the perception performance of the BLLS is tested again, and similar performance is still achieved. The experiments have proved (preliminarily) that the BLLS can be deployed underwater for a considerable time, and its perception ability won't be easily impaired.

4. Application Demonstration of the BLLS

A variety of underwater application requires identifying underwater objects and obtaining their motion parameters. In order to investigate the perceiving capability of the BLLS, a series of experiments are carried out in a test basin (6.0 m × 4.0 m × 1.6 m), as shown in **Figure 4**a. Above the surface of water is a guide rail, which is capable of moving in all direction at desired speed. The BLLS is deployed at the bottom of the basin to detect underwater (moving) objects, and different objects are mounted onto the guide rail to perform specified motion. Underwater camera is also deployed to capture the movement of the underwater object.

Figure 4b shows the schematic diagram of the BLLS perceiving a robotic fish. Figure 4c plots the open-circuit voltage output of the BLLS at different distances from the robotic fish. The open-circuit voltage signal generated by the BLLS gradually decreased to 4.2 mV as the fish moved (horizontally) from right above the BLLS to 8.0 cm away from the BLLS. A linear fitting to the BLLS yields a relationship of $U = -0.759L + 10.124$ with a linear

correlation coefficient of $R^2 = 0.99707$. It indicates that the perceiving effect of the BLLS is decreasing with the distance from the object.

Figure 4d demonstrates the open-circuit voltage signal generated by the BLLS as the robotic fish passes by at different speeds. It can be seen that the open-circuit voltage signal of the BLLS is ≈4.7 mV when the robot fish moves at a speed of 530.0 mm s⁻¹. The open-circuit voltage of the BLLS increases to ≈10.1 mV as the speed of the robotic fish increases to 600.0 mm s⁻¹. In the experiments, the speed of the robotic fish can also be roughly calculated using the time when the open-circuit voltage of the BLLS reached the peak, as shown in Figure 4e. The phase difference between the signals from the robot fish at the speed of 600.0 mm s⁻¹ and that from the speed of 590.0 mm s⁻¹ is ≈0.23 s. As the robot fish swimming speed further decreased to 560.0 and 530.0 mm s⁻¹, the phase difference of the BLLS signals became even larger, reflecting the speed difference.

To investigate how well the BLLS perceives (passing) underwater objects, the BLLS are tested with robotic seal, robotic fish, and ROV, as shown in Figure 4f and Movie S1 (Supporting Information). As the robot seal passes over the BLLS, the BLLS yields two (consecutive) crests. The larger cross-sectional area of the robotic seal's tail makes the second wave crest higher than the first. Due to the small size of the robotic fish, only one crest signal appeared as it passed over the BLLS. However, the BLLS produces a falling waveform followed by a rising waveform as the ROV passes by. The signal waveforms generated by the BLLS yield adequate differentiation for different objects underwater.

In Figure 4g, an experimental investigation is conducted using the ROV passing over the BLLS at different heights. In the
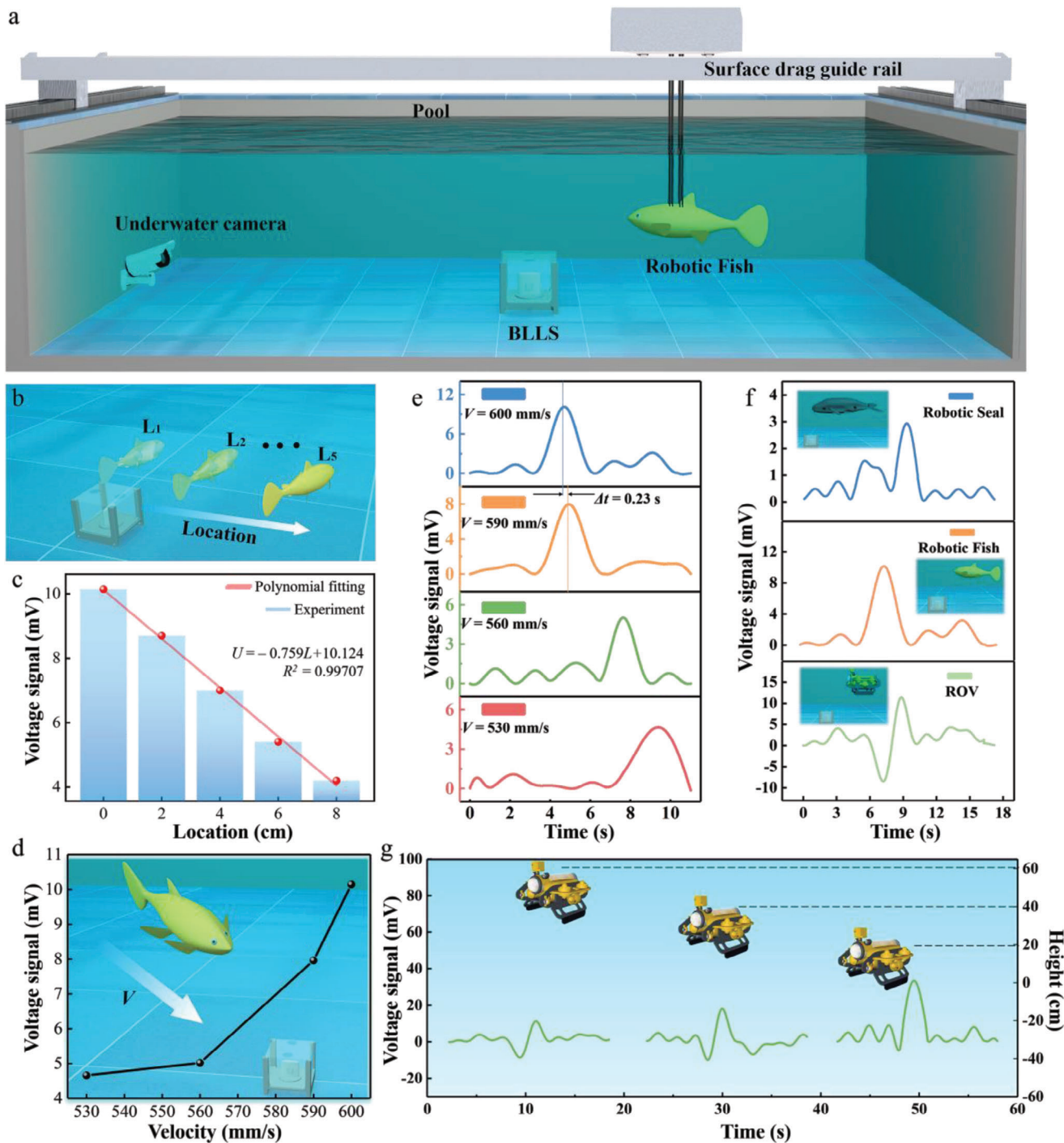
Figure 4. The BLLS perceiving underwater targets. a) The experimental setup. b) Schematic of the different positions of the robotic fish from BLLS. c) The open-circuit voltage of the BLLS with respect to the position of the robotic fish. d, e) The open-circuit voltage of the BLLS with respect to the speed of the robotic fish. f) The signal when the BLLS is detecting different objects. g) The open-circuit voltage of the BLLS with respect to the passing heights of the ROV.

experiment, the ROV starts at a height of 60.0, 40.0, and 20.0 cm directly above the BLLS and passes over the BLLS. The voltage signal from the BLLS gradually increased as the ROV descended from a height of 60.0–20.0 cm. It is possible to roughly identify the height of the ROV when it passes the BLLS. Through the object detection demonstration of the BLLS, we believe that the BLLS has the ability to perceive the underwater objects.

A single sensor is not sufficient for monitoring the underwater objects. Therefore, the BLLS sensors are arranged to form a perceiving grid (as shown in Figure S7 (Supporting Information)).
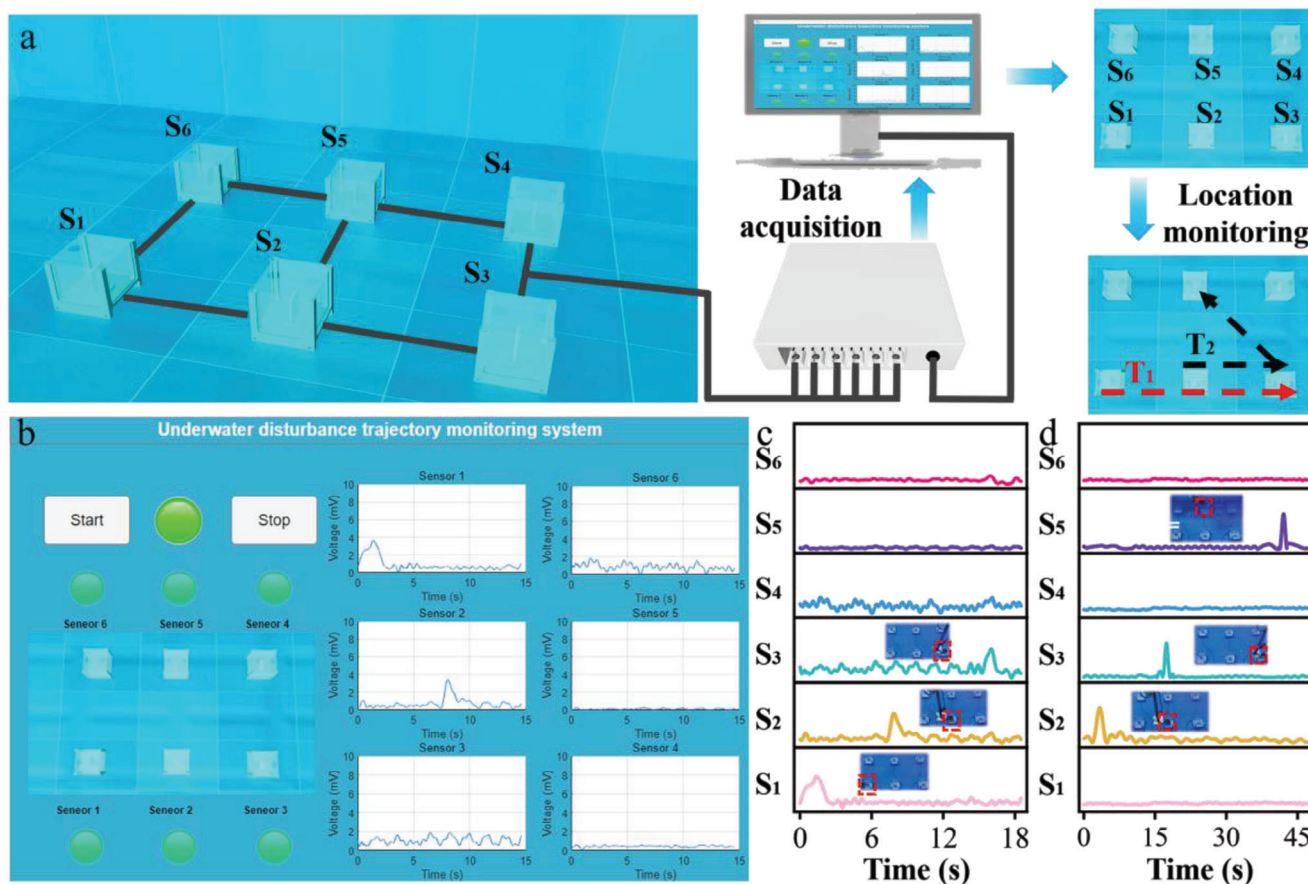
Figure 5. The BLLS in disturbance source trajectory profiling. a) Logic block of the disturbance source trajectory displaying. b) The display interface. c) Linear trajectory monitoring by the BLLS. d) Angular trajectory monitoring by the BLLS.

Figure 5a shows the working process of the perceiving grid. A multi-channel data acquisition device was installed to collect the data from the BLLS. The signals from the BLLS grid were transmitted in real time to a display interface developed in MATLAB. The interface will display the disturbance parameter as well as the movement trajectories of the disturbance sources (trajectory T1 and T2 in Figure 5a) as shown in Figure 5b. The left half of the panel shows the schematic diagram of the BLLSs array. The threshold voltage of the BLLSs No. 1–6 have been set in the system. When a BLLS perceives an external disturbance, the corresponding alert lamp will light up. The right half of the panel reflects the real-time voltage signals of each BLLS, through which one can observe the moving trajectory of the disturbance source. As shown in Figure 5c, when the disturbance generator moves from the BLLS No. 1 (S1) to the BLLS No. 2 (S2) and then to the BLLS No. 3 (S3), the sensors S1-S3 generate signals sequentially (the accompanying pictures are the position of the disturbance source). Movie S2 and Movie S3 (Supporting Information) shows real-time footage of the underwater disturbance trajectory measured by the grid. As can be seen, the cue lights of the S1-S3 BLLSs are triggered one after the another, as the disturbance source moves. Subsequently, the disturbance source was set to move in an angular route, as shown in Figure 5d. Figures S8 and S9 (Supporting Information) show the position movement status of two different trajectories. The speed of the disturbance source can also be deduced from the time sequence of the BLLS signal.

5. Conclusion

In this study, a triboelectric nanogenerator based sensor for dynamic pressure is proposed as a perceiving alternative underwater, especially when sonic/optical method are impaired. Imitating the mechanism of the fish lateral line, the sensor developed has the advantages of high sensitivity, good adaptability and (relative) low cost, which are favorable for large-scale deployment and long-term operation underwater. When the BLLS is subjected to external disturbance, the dielectric material and electrode material inside the sensing unit gets contact, thus generating an electrical signal. In the experiment, it is proved that the BLLS has the optimal perception effect when the angle of attack is 90°. It demonstrates its perception ability to the disturbance distance and disturbance frequency, and the linear correlation coefficients are greater than 0.99. In addition, the measured data from the BLLS could be analyzed to identify type, speed, position and trajectory of underwater objects. The BLLS will prove significant in forming a new underwater perceiving method, which could back-up the sonic/optical sensors in complex underwater environments.

6. Experimental Section

Fabrication of BLLS: The fabrication process of the BLLS is shown in Figure S10 (Supporting Information). PLA material was selected to fabricate the base and connection disk through a 3D printer. Ecoflex20 silicone rubber was selected as the encapsulating material for BLLS. Ecoflex20 consists of Part A and Part B. In the experiment, 150 mL each of Part A and Part B were put into a petri dish and mixed them. They were then placed in a vacuum pump for 3 min at 0.1 MPa. Following that, they were filled into the mold for the sensing unit and placed in a drying oven for 3 h. Subsequently, the sensing unit was encapsulated in silica gel, and liquid sealant was used to seal the sensing unit to make it waterproof. Finally, the sensing unit was fixed to the connection plate. The acrylic plate and the base were connected by bolts, and the interface was sealed with acrylic adhesive for reinforcement.

Performance Measurement and Characterization: In the performance test of the BLLS, the experimental platform was built using a linear motor (LINMOT EI200-P01), and the picture of the experimental platform is shown in Figure S11 (Supporting Information) of the supporting materials. A Keithley (6514) electrostatic meter was used to measure the voltage signal. A NI-6259 data acquisition card was chosen to collect the data from the BLLS. Control and real-time data acquisition were realized by LabVIEW software

Supporting Information

Supporting Information is available from the Wiley Online Library or from the author.

Conflict of Interest

The authors declare no conflict of interest.

Data Availability Statement

The data that support the findings of this study are available from the corresponding author upon reasonable request.

[1] D. Q. Huy, N. Sadjoli, A. B. Azam, B. Elhadidi, Y. Cai, G. Seet, *Ocean Eng.* **2023**, *267*, 113202.

[2] M. Asadnia, A. G. P. Kottapalli, Z. Shen, J. Miao, M. Triantafyllou, *IEEE Sens. J.* **2013**, *13*, 3918.

[3] A. Ghysen, C. Dambly-Chaudière, *Genes Dev.* **2007**, *21*, 2118.

[4] S. Hidaka, K. Ishii, K. Watanabe, presented at Int. Conf. on Artificial Life and Robotics (ICAROB 2017), Seagaia Convention Center, Miyazaki, Japan, January **2017**.

[5] Y. Yang, J. Chen, J. Engel, S. Pandya, N. Chen, C. Tucker, S. Coombs, D. L. Jones, C. Liu, *Proc. Natl. Acad. Sci. U.S.A.* **2006**, *103*, 18891.

[6] Z. Fan, J. Chen, J. Zou, D. Bullen, C. Liu, F. Delcomyn, *J. Micromech. Microeng.* **2002**, *12*, 655.

[7] R. Venturelli, O. Akanyeti, F. Visentin, J. Ježov, L. D. Chambers, G. Toming, J. Brown, M. Kruusmaa, W. M. Megill, P. Fiorini, *Bioinspir. Biomim.* **2012**, *7*, 036004.

[8] X. Zheng, A. M. Kamat, A. O. Krushynska, M. Cao, A. G. P. Kottapalli, *Adv. Funct. Mater.* **2022**, *32*, 2207274.

[9] P. Xu, J. Liu, X. Liu, X. Wang, J. Zheng, S. Wang, T. Chen, H. Wang, C. Wang, X. Fu, G. Xie, J. Tao, M. Xu, *npj Flexible Electron.* **2022**, *6*, 25.

[10] X. Zheng, A. M. Kamat, M. Cao, A. G. P. Kottapalli, *Adv. Sci.* **2023**, *10*, 2203062.

[11] J. C. Montgomery, S. Coombs, C. F. Baker, *The Biology of Hypogean Fishes*, Springer, Berlin **2001**, 87.

[12] E.-S. Hassan, in *The Mechanosensory Lateral Line: Neurobiology and Evolution*, Springer, Berlin **1989**, 217.

[13] Z. Tang, H. Feng, J. Lei, J. Lu, Z. Wang, B. Fu, W. Chen, *Int. J. Adv. Robot. Syst.* **2019**, *16*, 1729881418824826.

[14] Nannan Chen, C. Tucker, J. M. Engel, Yingchen Yang, S. Pandya, Chang Liu, *J. Microelectromech. Syst.* **2007**, *16*, 999.

[15] M. Asadnia, A. G. P. Kottapalli, J. Miao, M. E. Warkiani, M. S. Triantafyllou, *J. R. Soc., Interface* **2015**, *12*, 20150322.

[16] X. Hu, Z. Gong, Z. Ma, K. Wanig, D. Zhang, Y. Jiang, presented at *21st Int. Conf. on Solid-State Sensors, Actuators and Microsystems (Transducers)*, Orlando, FL, U.S.A, June **2021**.

[17] A. Kottapalli, M. Asadnia, J. Miao, M. Triantafyllou, presented at 28th IEEE Int. Conf. on Micro Electro Mechanical Systems (MEMS), Estoril, Portugal January **2015**.

[18] C. Wu, A. C. Wang, W. Ding, H. Guo, Z. L. Wang, *Adv. Energy Mater.* **2019**, *9*, 1802906.

[19] B. Chen, W. Tang, Z. L. Wang, *Mater. Today* **2021**, *50*, 224.

[20] Y. Wang, X. Liu, Y. Wang, H. Wang, H. Wang, S. L. Zhang, T. Zhao, M. Xu, Z. L. Wang, *ACS Nano* **2021**, *15*, 15700.

[21] X. Liang, S. Liu, S. Lin, H. Yang, T. Jiang, Z. L. Wang, *Adv. Energy Mater.* **2023**, *13*, 2300571.

[22] H. Yu, Z. Xi, Y. Zhang, R. Xu, C. Zhao, Y. Wang, X. Guo, Y. Huang, J. Mi, Y. Lin, T. Du, M. Xu, *Nano Energy* **2023**, *107*, 108182.

[23] H. Qiu, H. Wang, L. Xu, M. Zheng, Z. L. Wang, *Energy Environ. Sci.* **2023**, *16*, 473.

[24] L. Liu, Q. Shi, C. Lee, *Nano Energy* **2020**, *76*, 105052.

[25] C. Zhu, M. Wu, C. Liu, C. Xiang, R. Xu, H. Yang, Z. Wang, Z. Wang, P. Xu, F. Xing, H. Wang, M. Xu, *Adv. Energy Mater.* **2023**, *13*, 2301665.

[26] P. Xu, X. Wang, S. Wang, T. Chen, J. Liu, J. Zheng, W. Li, M. Xu, J. Tao, G. Xie, *Research* **2021**, *2021*, 9864967.

[27] J. Liu, P. Xu, J. Zheng, X. Liu, X. Wang, S. Wang, T. Guan, G. Xie, M. Xu, *Nano Energy* **2022**, *101*, 107633.

[28] P. Xu, J. Zheng, J. Liu, X. Liu, X. Wang, S. Wang, T. Guan, X. Fu, M. Xu, G. Xie, Z. L. Wang, *Research* **2023**, *6*, 0062.

[29] S. Wang, P. Xu, X. Wang, J. Zheng, X. Liu, J. Liu, T. Chen, H. Wang, G. Xie, J. Tao, M. Xu, *Nano Energy* **2022**, *97*, 107210.

[30] H. Zhao, M. Xu, M. Shu, J. An, W. Ding, X. Liu, S. Wang, C. Zhao, H. Yu, H. Wang, C. Wang, X. Fu, X. Pan, G. Xie, Z. L. Wang, *Nat. Commun.* **2022**, *13*, 3325.

[31] C. Zhao, D. Liu, Y. Wang, Z. Hu, Q. Zhang, Z. Zhang, H. Wang, T. Du, Y. Zou, H. Yuan, X. Pan, J. Mi, M. Xu, *Nano Energy* **2022**, *94*, 106926.

[32] X. Wang, J. Liu, S. Wang, J. Zheng, T. Guan, X. Liu, T. Wang, T. Chen, H. Wang, G. Xie, P. Xu, J. Tao, M. Xu, *Adv. Mater. Technol.* **2022**, *7*, 2101098.

**ADVANCED
SCIENCE NEWS**

www.advancedsciencenews.com

**NANO · MICRO
small**

www.small-journal.com

[33] J. An, Z. Wang, T. Jiang, P. Chen, X. Liang, J. Shao, J. Nie, M. Xu, Z. L. Wang, *Mater. Today* **2020**, *41*, 10.

[34] Y. Li, C. Liu, H. Zou, L. Che, P. Sun, J. Yan, W. Liu, Z. Xu, W. Yang, L. Dong, L. Zhao, X. Wang, G. Wang, Z. L. Wang, *Cell Rep. Phys. Sci.* **2023**, *4*, 101191.

[35] X. Liang, S. Liu, Z. Ren, T. Jiang, Z. L. Wang, *Adv. Funct. Mater.* **2022**, *32*, 2205313.

[36] Y. Yang, X. Guo, M. Zhu, Z. Sun, Z. Zhang, T. He, C. Lee, *Adv. Energy Mater.* **2023**, *13*, 2203040.

[37] X. Guo, T. He, Z. Zhang, A. Luo, F. Wang, E. J. Ng, Y. Zhu, H. Liu, C. Lee, *ACS Nano* **2021**, *15*, 19054.

[38] Q. Shi, H. Wu, H. Wang, H. Wu, C. Lee, *Adv. Energy Mater.* **2017**, *7*, 1701300.

[39] Z. Che, S. O'donovan, X. Xiao, X. Wan, G. Chen, X. Zhao, Y. Zhou, J. Yin, J. Chen, *Small* **2023**, 2207600.

[40] X. Wang, Y. Shi, P. Yang, X. Tao, S. Li, R. Lei, Z. Liu, Z. L. Wang, X. Chen, *Small* **2022**, *18*, 2107232.

[41] K. Lee, S. Mhin, H. Han, O. Kwon, W.-B. Kim, T. Song, S. Kang, K. M. Kim, *J. Mater. Chem. A* **2022**, *10*, 1299.

[42] L. Zhao, Q. Zheng, H. Ouyang, H. Li, L. Yan, B. Shi, Z. Li, *Nano Energy* **2016**, *28*, 172.

[43] S. Schuster, *Curr. Biol.* **2008**, *18*, R176.

[44] Q. Wang, P. Xiao, W. Zhou, Y. Liang, G. Yin, Q. Yang, S.-W. Kuo, T. Chen, *Nano-Micro Lett.* **2022**, *14*, 62.

[45] Y. Yang, N. Nguyen, N. Chen, M. Lockwood, C. Tucker, H. Hu, H. Bleckmann, C. Liu, D. L. Jones, *Bioinspir. Biomim.* **2010**, *5*, 016001.

[46] J. Song, R. G. Northcutt, *Brain Behav. Evol.* **1991**, *37*, 24.

[47] J. C. Liao, *Biol. Lett.* **2010**, *6*, 402.